Available online at www.sciencedirect.com
ScienceDirect
Journal of Hazardous Materials 155 (2008) 230–242
Journal of Hazardous Materials
www.elsevier.com/locate/jhazmat

Adsorptive, thermodynamic and kinetic performances of Al/Ti and Al/Zr-pillared clays from the Brazilian Amazon region for zinc cation removal

Denis L. Guerra [a], Claudio Airoldi [a,*], Vanda P. Lemos [b], Rômulo S. Angélica [b]

[a] *Instituto de Química, Universidade Estadual de Campinas, Caixa Postal 6154, 13084-971 Campinas, São Paulo, Brazil*
[b] *Universidade Federal do Pará, Centro de Geociência, Caixa Postal 1611, 66075-110 Belém, Pará, Brazil*

Received 2 May 2007; received in revised form 14 November 2007; accepted 15 November 2007
Available online 22 November 2007

Abstract

Smectite clay samples from the Amazon region, Brazil, were pillarized by intercalating the species obtained from the chemical reactions: (i) $AlCl_3{\cdot}6H_2O$/NaOH, (ii) titanium ethoxide in hydrochloric acid and (iii) direct use of $ZrOCl_2{\cdot}8H_2O$ solution. The natural matrices and the pillaring solutions were maintained under vigorous stirring at 298 K for 3 h and then subjected to calcination at temperatures of 723 and 873 K. Natural and pillared matrices were characterized by XRD, FTIR, TG–DTG and nitrogen adsorption–desorption isotherms. The resulting materials were used for zinc adsorption from aqueous solution at room temperature. The Langmuir, Freundlich and Temkin adsorption isotherm models have been applied to fit the experimental data and the Freundlich model is limited for higher concentrations. The pillaring process increases the thermal stability, the basal spacing of the natural clay sample (A_1) from 1.55 to 2.06 nm and the surface area from 44.30 to 223.73 $m^2\,g^{-1}$. Kinetic studies demonstrated an equilibrium time of 180 min for zinc adsorption on the pillared matrices. Pseudo-first-order, Lagergren pseudo-second-order and Elovich equations demonstrated a better agreement with second-order kinetics was obtained with $K_2 = 4.17–10.43 \times 10^{-3}$ g mg^{-1} min^{-1} for the A_1 sample.

Keywords: Pillared clay; Adsorption; Smectite; Zinc; Kinetics

1. Introduction

Industrial activities generate a wide diversity of wastewaters with contaminants that can harm ecosystems and human beings. To minimize the impact of industrial wastewaters, contaminant adsorption has often been used as an important approach for resolving such problems. In this context, many materials have been proposed and some of them are useful candidates, such as natural and modified clay surfaces [1].

Several classes of zeolite compounds have been used in adsorption processes for toxic metal removal from aqueous solution. Among a series of low-cost adsorbents, natural clay smectite with high adsorption or exchange capacity or its corresponding modified surfaces have been employed in many of these activities. Pillared clays, when employed for removal divalent copper, cobalt, nickel and zinc cations were also intensively investigated with the purpose of remediation of polluted water from industries, with excellent performance [1,2].

Nowadays, pillared interlayered clays (PILC) represent a new microporous generation, whose two-dimensional pores enable insertions, including large molecules in the cavities, with the advantage in maintaining catalytic selectivity properties for molecular reactions [3]. In principle, these kind of materials are synthesized through charge-compensating cations, by exchanging the original cation in the interlayer space of the swelled clays with different cations in polymeric forms, containing not only Al [2–7], Zr [8,9], Cr [10] and Ti [11–13], but also modified Al–P and mixed pillared Si–Al, Al–Ti and Al–Fe [14], etc. After

* Corresponding author. Tel.: +55 19 35213055; fax: +55 19 35213023.
E-mail address: airoldi@iqm.unicamp.br (C. Airoldi).

0304-3894/$ – see front matter © 2007 Elsevier B.V. All rights reserved.
doi:10.1016/j.jhazmat.2007.11.054

synthesis, the next step consisted in calcinating these inserted oxy-hydroxycationic polymers to yield rigid, thermally stable oxide species as pillars, with a layered clay structural arrangement, to prevent any collapse at high temperatures. Thus, the as-extracted clay material has the original cation conveniently exchanged to yield a new intercalated material, attached to the pillar after calcination. The main objective in pillaring clays is to achieve a basal spacing as large as possible, that operation contributes to the development of materials with large surface areas and volumes of pores, with specific properties, depending on the nature of the oxide included in the synthesized pillar [10–14].

The pillared interlayered clay structures are generally synthesized from the family of mineral smectites that includes beidellite, hectorite, fluorhectorite, saponite, sauconite, montmorillonite and nontronite. From the structural point of view, smectite clays are composed of layers with two sheets of silica sandwiched by an Al or Mg octahedral layer in a 2:1 structural arrangement. The substitution of some Al^{3+} by Mg^{2+} or Li^{+} cations or as occurs by isomorphous replacement of tetrahedral Si^{4+}, the negative charge inside the layers is compensated, in turn, by the presence of hydrated cations in this interlayer region [15–19].

The chemical surface and structural PILC properties establish the potentiality of applications, such as adsorbent or as catalyst. Presently, the latter process is illustrated in a wide range of reactions, such as: cracking, cyclohexane conversion, toluene in methanol alkylation, propylene oligomerization, etc. All these applications are also commonly employed in the petroleum industry for long-chain hydrocarbon filtering and azeotropic cracking [18,19].

The aim of the present investigation is to explore the structural and physical–chemical properties of two different types of smectites, natural and pillared clays. The pillaring processes were developed with intercalation of $Al_{13}O_4(OH)_{24}(H_2O)_{12}{}^{7+}$/$Ti(OC_2H_5)_4$ and $Al_{13}O_4(OH)_{24}(H_2O)_{12}{}^{7+}$/$ZrOCl_2{\cdot}6H_2O$. Various parameters related to the chemical compositions of the matrices, temperature of calcination, synthetic methodology to obtain PILC and zinc adsorption from aqueous solution at room temperature have been investigated. Langmuir, Freundlich and Temkin adsorption isotherm models were applied in order to fit the experimental data. Moreover, the effect connected to the variation of the texture of the PILC was analyzed by different techniques. In addition, a kinetic study was performed by considering the experimental data, which were adjusted to the pseudo-first-order Lagergren and pseudo-second-order and Elovich models.

2. Experimental

2.1. Raw material

The clays were sampled at the Sena Madurera area, State of Acre, Northern Brazil. Two different samples named A_1 and A_2 were separated by sedimentation. The cation-exchange capacity (CEC) was evaluated by employing ammonium acetate at pH 8, to give 1.12 and 1.30 mmol g^{-1} for the A_1 and A_2 clay samples, respectively.

2.2. Sample preparation

The samples were ground and passed through a USS sieve of 0.074 mm (200 mesh) and dried at 333 K to decrease humidity to the 12–15% range. X-ray powder diffractometry confirmed the presence of smectite clays by several conventional sample preparation procedures. For the preliminary analyses on natural samples three conventional procedures were employed: air-dried, ethylene glycol solvated and heated at 573 and 773 K.

2.3. Synthesis of the pillars

A basic solution of 0.20 mol dm^{-3} NaOH was slowly added to a 0.20 mol dm^{-3} aqueous $AlCl_3{\cdot}6H_2O$ solution to maintain the OH/Al molar ratio equal to 2 [1] under vigorous stirring at 333 K.

The zirconium solution was prepared by adding appropriate volumes of 0.10 mol dm^{-3} aqueous $ZrOCl_2{\cdot}8H_2O$ solution directly to clay suspension at room temperature with vigorous stirring [8,9].

Titanium intercalating solutions were obtained by slowly adding titanium ethoxide, $Ti(OC_2H_5)_4$, to 5.0 mol dm^{-3} hydrochloric acid solution under vigorous stirring at H^+/Ti molar ratio of 0.48 [11]. The suspension was aged under stirring at room temperature for 5 h.

The intercalating aluminum and titanium solutions were mixed in 1:1 proportion at room temperature, stirred for 4 h and identically applied to prepare the Al/Zr solutions.

The mixed polymeric Al/Ti or Al/Zr solutions were added dropwise to a suspension of 5% of natural clay samples A_1 or A_2 in a mixture 1:1 of deionized water and ethanol. The final solution containing polymeric ions and natural clay samples was filtered, washed with deionized water and the samples were calcinated at 723 and 873 K for 2 h, to give the pillared matrices Al/Ti-A_n-723/873 and Al/Zr-A_n-723/873 ($n = 1, 2$).

2.4. Adsorption

Samples of about 60 mg of the pillared clays suspended in 20.0 cm^3 of aqueous solution containing zinc at 298 ± 1 K were used to investigate the adsorption process. Firstly, natural and pillared adsorption samples were evaluated by varying the pH in the 1.0–5.0 range with addition of 0.10 mol dm^{-3} of nitric acid or 0.10 mol dm^{-3} sodium hydroxide.

The isotherms of concentration as functions of time, pH and the degree of adsorption were obtained through a batch method. Each isotherm can be obtained through the number of moles adsorbed per gram (N_f), calculated by the difference between the initial (n_i) and the number of moles of zinc remaining in the supernatant (n_s) divided by the mass (m) of the compound used, $N_f = (n_i - n_s)/m$. From these isotherms the time for surface saturation was used for all other determinations. In such condition the number of moles of cation adsorbed (N_f) increased with concentration in the supernatant (C_s) as a function of pH and

time (t), until the plateau related to total saturation of the acid center in the layered structure was obtained [5,20].

The most common model to adjust the adsorption is that proposed by Langmuir, originally derived for gas adsorption on planar surfaces such as glass, mica and platinum. The process has successfully been extended to heavy metal ions on porous surfaces. The quantity adsorbed is related to the equilibrium solution concentration of the adsorbate, after adjusting to K_L and b parameters from Eq. (1) and the plateau of the isotherm-derived K_L value by measuring the adsorbate on the surface. The value of b is the upper limit and represents the maximum adsorption, determined by the number of reactive surface sites by converting Eq. (1) into its linear form [5,20]:

$$\left[\frac{C_s}{N_f}\right] = \left[\frac{1}{K_L b}\right] + \left[\frac{C_s}{b}\right] \quad (1)$$

C_s/N_f and the distribution coefficient K_L, can be plotted against the concentration in the supernatant. If the Langmuir equation can be applied, the measured data should fall on a straight line with slope giving K_L and the intercept $K_L b$ values, $1/K_L b$ being the angular and $1/b$ the linear coefficients [5,20].

Another fitting for the adsorption process is established by the Freundlich equation:

$$N_f = K_f C^{1/n} \quad (2)$$

where K_f and n are adsorption capacity and affinity constants of the adsorbent. Although this equation was first empirically employed, it can be derived with the assumption of a continuous variation in thermal effect during the adsorption. There is no assurance that the derivation of the Freundlich equation is unique; consequently, if the collected data can fit to the equation, it is only likely, but not proven, that the surface is heterogeneous. The Freundlich model unfortunately predicts both infinite adsorption at dilute concentration and a corresponding thermal effect related to the adsorption at zero coverage [5–20].

The Temkin equation was also applied for solid/liquid interface equilibrium:

$$N_f = A \ln C + B \quad (3)$$

where A and B are parameters of the equation, estimated by plotting N_f against $\ln C$. The values are obtained for A and B, being the angular and linear coefficients of the straight line, whose coefficients can be used to adjust the experimental data to the theoretical model.

2.5. Thermodynamic parameters

Thermodynamic parameters such as Gibbs free energy (ΔG), enthalpy (ΔH) and entropy (ΔS) for the adsorption of cations on pillared clays are calculated using the following equations [21,22]:

$$\Delta G = -RT \ln K_L \quad (4)$$

where K_L is the equilibrium constant obtained from Langmuir model, T the absolute temperature (K) and the universal gas constant $R = 8.314 \times 10^{-3}$ kJ K^{-1} mol^{-1}. The relationship between K and thermodynamic parameters of ΔH and ΔS can be described by the van't Hoff correlation in the following equation [21,22]:

$$\ln K_L = \frac{\Delta S}{R} - \frac{\Delta H}{RT} \quad (5)$$

The thermodynamic study was made at a constant pH value of 5.0 at three different temperatures 303, 318 and 333 K. This study used 3.0 g dm^{-3} clay, an interaction time of 200 min and an initial Zn(II) concentration of 50.0 cm^3 dm^{-3}.

2.6. Analytical procedures

X-ray powder diffraction (XRD) patterns were recorded with a Philips PW 1050 diffractometer using Cu Kα (0.154 nm) radiation in the region between 2° and 65° (2θ) at a speed of 2°/min and steps of 0.050°.

A potenciometric method was used to measure the surface charge density σ_0 (μC cm^{-2}) at different pH, by using a Systronic pH meter model 362μ to measure the pH of the solution.

For the infrared spectroscopy, the samples were oven-dried at 393 K to remove any adsorbed water. Each sample of about 1.3 mg was finely ground for 1 min, combined with 100 mg of oven-dried spectroscopic grade KBr and pressed with 7 tonnes into a disc under vacuum. The spectra of each sample was recorded in triplicate between 400 and 4000 cm^{-1} by accumulating 64 scans at 4 cm^{-1} resolution, using a Perkin-Elmer 1760X Fourier transform infrared spectrometer.

Thermal analysis, differential thermal analysis–thermogravimetry (DTA–TG) was carried out in a Stanton Redcroft 1000/1500 instrument coupled to a DC and temperature controller. Data from DTA and TG were obtained in all cases at a heating rate of 0.33 K s^{-1} between 313 and 1173 K under static air atmospheres.

BET (Brunauer–Emmett–Taller) surface areas and porosity measurements of the PILC samples were determined using a Quantachome/Nova Surface Area-Pore Volume Analyzer, model 1200/5.01. The mesopore size distribution was obtained by applying the BJH (Barret–Joyner–Halenda) method to the adsorption branch of the isotherm.

The natural A_1 and A_2 clay and mixed PILC samples were analyzed with induced coupled plasma-optical emission spectrometry (ICP-OES), using an ARL 34000 instrument. Oven-dried powdered samples weighing exactly 0.231, 0.254, 0.241 and 0.234 g, respectively, were placed separately on glass weighing dishes and transferred quantitatively to pre-cleaned nitric acid digestion bottles. The samples were then digested with 7.0 cm^3 of concentrated nitric and hydrochloric acids in 1:3 proportion in volume, with identical volume of hydrofluoric acid and allowed to stand for 5 days. The samples were cooled in an ice-bath and 25.0 cm^3 of boric acid was added with stirring, followed by 50.0 cm^3 of deionized water. The solution was then diluted to 100.0 cm^3. For each sample, a blank and a set of elemental standards were run to calibrate the ICP-OES instrument.

The samples of natural and pillared clays for scanning electron microscopy (SEM) and energy dispersive spectroscopy

Table 1
Elemental analyses of original and pillared clay samples

Sample	SiO_2 (%)	Al_2O_3 (%)	CaO (%)	Na_2O (%)	K_2O (%)	MgO (%)	Fe_2O_3 (%)	TiO_2 (%)	ZrO_2 (%)
A_1	69.78	16.89	2.68	2.31	3.92	1.47	2.95	–	–
A_2	69.76	16.90	2.98	3.09	2.89	1.40	2.98	–	–
Al/Zr-A_1-723	69.78	20.71	1.03	1.71	2.02	0.44	2.95	–	1.36
Al/Ti-A_1-723	69.78	20.51	1.94	0.17	1.01	1.27	2.94	2.37	–
Al/Zr-A_1-873	69.78	20.65	1.08	1.19	2.13	0.92	2.95	–	1.30
Al/Ti-A_1-873	69.78	21.45	1.07	1.08	1.99	0.42	2.94	1.27	–
Al/Zr-A_2-723	69.76	19.98	1.49	1.37	1.90	0.90	2.98	–	1.62
Al/Ti-A_2-723	69.76	20.13	1.98	1.03	1.56	0.48	2.98	2.08	–
Al/Zr-A_2-873	69.76	20.03	1.99	1.55	1.87	0.58	2.98	–	1.24
Al/Ti-A_2-873	69.76	19.99	1.14	1.15	1.78	0.95	2.98	2.25	–

(EDS) were prepared on orientated blades at 298 K and sputtered with gold. The instrument used was a model LEO-ZEISS, 430 Vp, in conditions of analysis, using secondary images obtained to 20 kV, with an experimental distance of 11 mm.

3. Results and discussion

3.1. Elemental analysis

Elemental analyses for the original and chemically modified clay samples gave the results listed in Table 1. These values are consistent with smectite, with aluminum being the major clay mineral contained in the structure. The pillared clay samples presented beyond silicon other major components aluminum, zirconium and titanium, followed by calcium, potassium, magnesium and sodium, in agreement with the attachment of these elements on the original smectite structure. The composition of the original smectite samples was calculated through the chemical analysis, to give the formulae:

- A_1: $(Na_{0.27}K_{0.30})(Al_{1.19}Mg_{0.13}Fe_{0.14}Ca_{0.17})(Si_4O_{10})(OH)_2$
- A_2: $(Na_{0.16}K_{0.23})(Al_{1.19}Mg_{0.27}Fe_{0.13}Ca_{0.18})(Si_4O_{10})(OH)_2$

The resulting formulae represent smectite montmorillonite, whose structure is formed by four tetrahedral silicon atoms, suggesting the presence of silicon in amorphous form in the matrix or the possibility of isomorphic substitution on the net crystalline matrix [18].

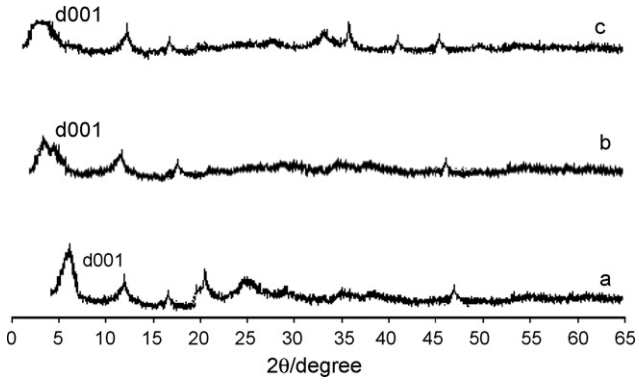

Fig. 1. X-ray patterns of natural A_1 (a), pillared Al/Zr-A_1-723 (b) and Al/Ti-A_1-873 (c) clays calcinated at 723 and 873 K.

3.2. X-ray powder diffraction

The total mineralogical composition of the starting materials, represented by A_1 and A_2 clay samples, exhibited mainly hematite and goethite components [18], but with the possible existence of a reduced amount of kaolinite.

The X-ray diffraction patterns found for d_{001} are listed in Table 2. Natural A_1 and pillared Al/Zr-PILC and Al/Ti-PILC clays, are illustrated as examples in Fig. 1. An increase in the interlayer distances after the pillaring process was observed, by changing d_{001} from 1.554 to 2.064 nm for pillared samples, respectively, after calcinating at 723 K. It was also observed that the Al/Zr-PILC samples presented a slightly broader peak,

Table 2
Basal spacing and textural proprieties of smectite and aluminum-pillared samples, pH, the basal space (d_{001}), surface area (S), micropore area (M_a), crystallinity (C_y), average pore diameter (P_d) and pore volume (P_v) for natural and pillared clay samples

Sample	pH_{zpc}	d_{001} (nm)	S ($m^2\,g^{-1}$)	M_a ($m^2\,g^{-1}$)	C_y	P_d (nm)	P_v ($cm^3\,g^{-1}$)
A_1	7.48	1.554	44.30	18.21	0.90	2.5	0.12
A_2	7.26	1.548	41.20	17.65	0.91	2.2	0.11
Al/Zr-A_1-723	3.95	2.064	223.73	27.18	0.78	4.3	0.20
Al/Ti-A_1-723	3.98	1.956	177.56	20.03	0.75	4.1	0.19
Al/Zr-A_1-873	3.85	1.961	198.13	25.48	0.68	4.2	0.21
Al/Ti-A_1-873	3.99	1.880	178.40	19.88	0.70	3.9	0.22
Al/Zr-A_2-723	3.97	1.949	198.40	28.70	0.72	4.0	0.22
Al/Ti-A_2-723	3.87	1.905	168.98	19.87	0.78	4.0	0.19
Al/Zr-A_2-873	3.94	1.896	177.70	24.47	0.68	4.3	0.19
Al/Ti-A_2-873	3.97	1.864	143.90	17.81	0.61	3.9	0.18

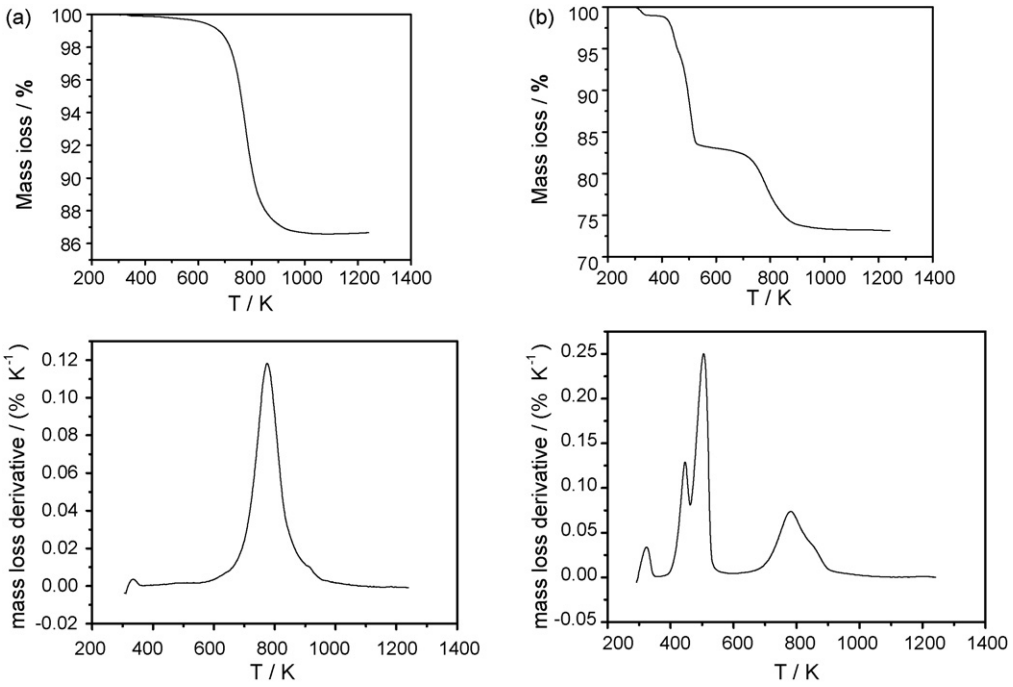

Fig. 2. Thermogravimetric and differential curves for natural A_1 (a) and Al/Zr-A_2-878 (b) samples.

in comparison with Al/Ti-PILC, reflecting differences in the degree of crystallinity, calculated from the Biscaye equation [13], as shown in Table 2, whose difference can be related to the elemental interferences in the pillaring process. This fact can be explained through the hypothesis of the existence of different species in the interlayer region that make the entrance of the intercalation ion difficult, resulting in structural distortions. However, another possibility is the inadequate adjusting of the ion in the interlayer region. When the matrix is submitted to the high temperatures of calcination, premature dehydroxylation of pillars in a given interlayer region results in a partial pillaring process. Well-pillared samples showed approximately the same d_{001} basal spacing in all cases. The great influence of the number of pillars in the interlayer spacing on the constitution and distribution of the pillars has been previously reported [14].

3.3. Thermogravimetry

The thermogravimetric curves and the derivative curves are depicted in Fig. 2. These were obtained after the natural A_1 and Al/Zr-PILC and Al/Ti-PILC clay samples were equilibrated in a desiccator at room temperature. The natural sample presented mass loss in only one step from 600 to 1000 K, as clearly indicated by the derivative curve, showing only one simple peak, although a small mass loss at a lower temperature, related to humidity, gave a small peak near 340 K, also indicated in the corresponding derivative curve. Identically, the pillared matrices presented at low temperature from 300 to 370 K, a mass loss due to humidity. From this stage three other mass losses in the 400–470, 470–600 and 600–950 K intervals are observed, which are confirmed by the set of three peaks in the derivative curve. The first stage can be attributed to hydrating water, whereas the second step is due to dehydroxylation of the silicate structure. For aluminum and magnesium pillared materials, the net isomorphic substitution in the clay with different bonding strengths between the oligocations and the surrounding oxygen (or hydroxyl) ions can be observed. Dehydroxylation continues smoothly from 950 to 1200 K, related to the stability of pillars. An important decrease in the basal spacing values occurs at this temperature interval, suggesting the collapse of the original clay structure. Therefore, the thermogravimetric data are in agreement with the aforementioned thermal stability of the synthesized pillared clay up to 873 K.

3.4. Infrared spectroscopy

Similar infrared spectra of natural and pillared aluminum samples calcinated at 723 K are shown in Fig. 3. However, the latter presented a small, low intensity band at 667 cm^{-1}, which band is shown in the expanded spectrum in Fig. 3c. This lattice vibration can be ascribed to the Al–O bond of the coordinated aluminum in a tetrahedral environment in the structure located in the center of the aluminum pillars. The infrared spectra for natural clays presented bands in the 1787–1740 cm^{-1} region that are attributed to hydrating water. Similar results were previously reported [6], using $Al(NO_3)_3$ as pillaring source.

The infrared spectra for pillared samples presented broad bands at 3774 cm^{-1} related to the OH moiety of the SiOH group, corresponding to free silanol groups, which are located on silica or on the external surfaces of the zeolite structure [6,23]. Such hydroxyls can be sited at the corners and fractures of sheets or are formed by tetrahedral inversion processes. The new bands at

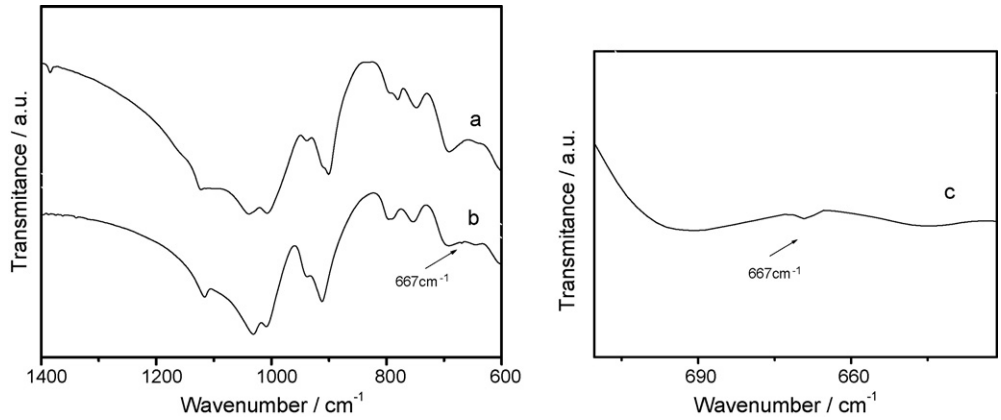

Fig. 3. Infrared spectroscopy natural (a) and Al/Zr-A_2-878 (b) samples, denoting the Al–O bond formed. The expanded Al/Zr-A_2-878 spectrum is shown in (c).

3742, 3735 and 3756 cm^{-1} are probably produced by the change of position of the SiOH group in the structure of the smectite. This original position can be altered by the entrance of the intercalated ion in the smectite structure, which is likely to be due to silanol species in the pillars, similar results were previously reported [6,23]. However, this result was not observed for pillared clays calcinated at temperatures above 973 K, a fact that can be associated with the occurrence of pillar structure dehydroxylation. A weak shoulder at 3715 cm^{-1} is observed in all clays, which is characteristic of isolated hydroxyl groups on octahedral aluminum in the Al_2O_3 structure. A similar interpretation was previously reported [30], but involving cations in the octahedral sheet and also possibly in pillars, as observed with the Al-pillared clay samples. Accordingly, the hydroxyl species is also identified as a $Al^{VI}OH$ species [6], as shown in Fig. 4.

The pillared materials have properties in adsorbing pyridine, this probe molecule can be followed by infrared spectroscopy to detect the relative intensity of the pyridinium ions bands at 1545 cm^{-1}, in addition to the pyridine coordinated to Lewis sites at 1454 cm^{-1}, as shown in Fig. 5. Thus, Al/Ti-PILC presented Brønsted and Lewis acid sites after degassing in vacuum (1.33×10^{-3} Pa) at 573 K. The intensity of the Brønsted band was reduced at 723 K and pyridine was sorbed predominantly on Lewis acid sites. The Al/Zr-PILC materials showed the most intense bands in comparison with those obtained with Al/Ti-PILC after adsorption process. This fact can be explained by the hypothesis of the existence of different species in the interlayer region during the pillarization process. The spectrum of natural smectite showed small intense bands in the pyridine adsorption region, demonstrating deficiencies in the adsorption process with pyridine, as illustrated in Fig. 5b.

3.5. Textural analysis

The textural results with pillared clays are listed in Table 2. All isotherms correspond to type IV of the BDDT (Brunauer, Deming, Deming and Teller) classification [7,24] and reflected a microporous network formed in the interlayer, with well-defined H4 hysteresis loops, in agreement with de Boer's classification, [24] related to micropores, with capillaries due to the interlayer

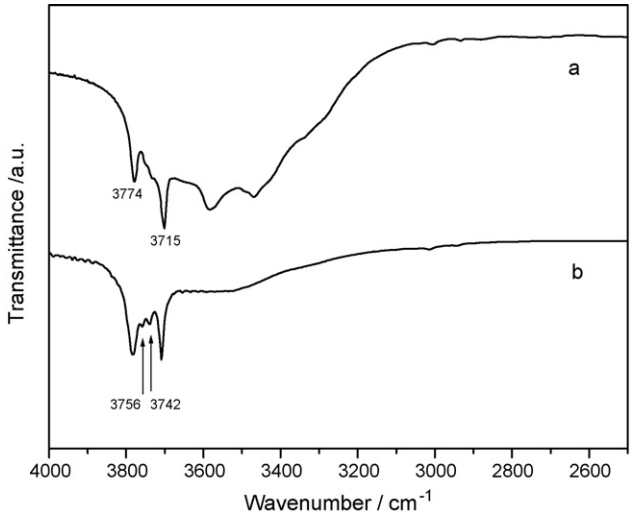

Fig. 4. Infrared spectra of natural sample: A_2 (a) and pillared clay sample: Al/Zr-A_2-873 (b).

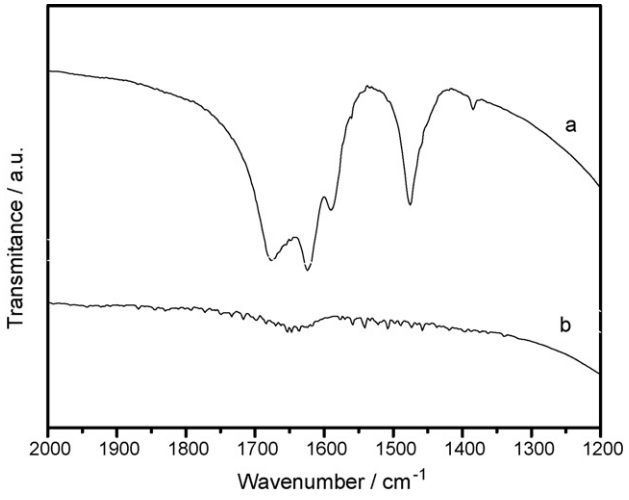

Fig. 5. Infrared spectra of pyridine adsorbed on Al/Zr-A_1-723 (a) and natural A_1 (b) samples.

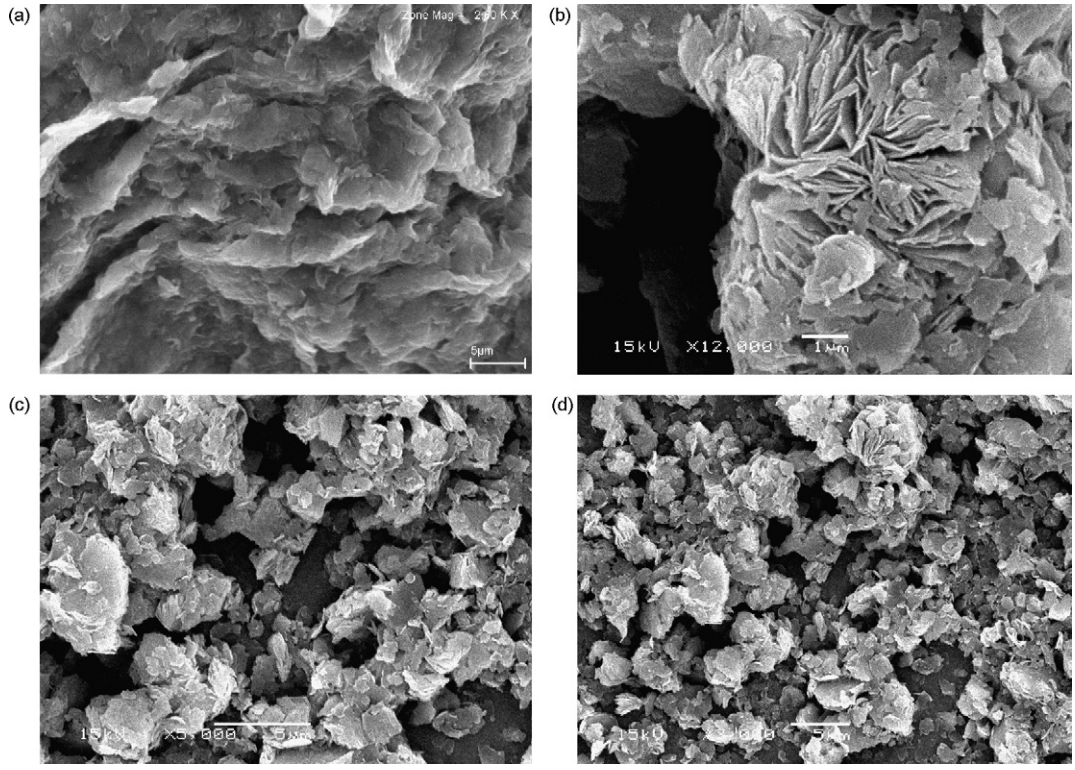

Fig. 6. Scanning electron microscopy for natural A_1 (a) and A_2 (b), and pillared Al/Zr-A_1-723 (c) and Al/Zr-A_2-723 (d) samples.

space between parallel walls of aluminosilicate units. The values of surface area and volume of micropores after application of the data of the BET equation and the BJH method along with the H–J standard curve are also included in Table 2, which presents $V_{0.98}$, which corresponds to the total pore volume reached at $P/P_0 = 0.98$.

Pore size distributions in the pillared sample series varied depending on the raw material source and particle size. Thus, pillared clays showed unimodal distribution with pore sizes and natural clay samples gave bimodal distributions.

3.6. Scanning electron microscopy

The results of scanning electron microscopy for the pillared Al/Zr-A_1-723 matrix confirmed the pillaring process with aluminum, titanium and zirconium, without producing any change in the crystal form and crystalline size of the original smectites. For all experiments the smectite remained in the primitive crystal form, presenting itself in the foliated stage with illite crystals in the extremities, as shown in Fig. 6. The surface morphologies of natural clays A_1 and A_2 and Al/Zr-A_1-723 are different from that of Al/Zr-A_2-723. The natural matrix samples appeared as corn flake-like crystals with a fluffy appearance revealing its extremely fine plate-like structure. After the pillaring process with mixed oxide pillars, the natural matrix has become more porous and fluffy. This porous and fluffy appearance probably occurred due to the charges on the surface that correspond to those of the particles, as a result of pillaring and reduction in certain amorphous regions, originally associated with natural clay, as observed before [25].

3.7. Determination of the zero point of charge

The zero point of charge of the natural and mixed PILC clay samples was determined by values of σ_0 obtained through potentiometric titration, by using the following equation [25]:

$$\sigma_0 = \frac{F(C_A - C_B + [OH^-] - [H^+])}{A} \quad (6)$$

where F is Faraday's constant, C_A and C_B are the concentration of strong acid or base after each addition during titration, $[OH^-]$ and $[H^+]$ are the equilibrium concentrations of these ions bonded to the surface and A is the clay surface area. The plots of σ_0 versus pH values for natural and pillared clay samples are shown in Fig. 7.

The point of interception of σ_0 with pH_{zpc} after mixed pillaring indicated that the surface became more negative and this result aided adsorption of positively charged species such as Zn(II) ions through electrostatic interaction. A variation in textural properties, cation exchange capacity and density was also observed after the pillaring process.

3.8. Metal adsorption

The pH of the aqueous solution is an important controlling parameter in the adsorption process. The influence of the pH values on concentration by natural and pillared clays, represented by the number of moles adsorbed, N_f, is plotted in Fig. 8, showing that the exchange of metal ions strongly decreases with the acidity of the solution. Obviously, a pH value 5.0 is opti-

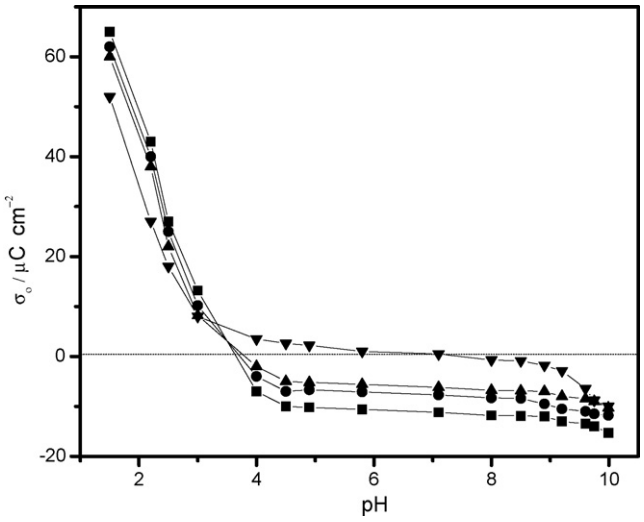

Fig. 7. Potentiometric titration curves depicting the surface charge as a function of pH variation for natural A_1 (▼) and pillared Al/Zr-A_1-823 (■); Al/Ti-A_1-723 (▲); and Al/Zr-A_1-723 (●) samples.

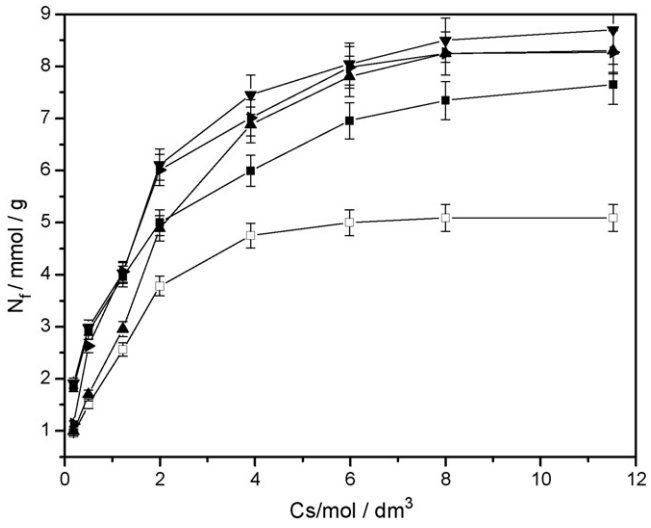

Fig. 9. Zinc adsorption on pillared clay samples (3.0 g dm^{-3} clay, initial Zn(II) concentration 50.0 mg dm^{-3}, pH 5.0, controlled temperature 298 ± 1 K) A_1(□), Al/Zr-A_1-723 (▲); Al/Ti-A_2-723 (■); Al/Zr-A_2-723 (►); and Al/Ti-A_1-723 (▼).

mal for the adsorption of metal ions. Exchange experiments at higher than 5.0 were not carried out due to the risk of hydrolysis [26–30].

The adsorption results obtained with zinc cations on natural and pillared clay samples are shown in Fig. 9, with a clear demonstration the increase of the amount adsorbed, N_f, as the pillarization increased, when compared with the original clay. The results of the applied Langmuir, Freundlich and Temkin models of adsorption are shown in Fig. 10 for Al/Zr-A_2-723 and were performed for all pillared and the original clays. These parameters are listed in Table 3. These values are in agreement with the three possible models of adsorption and they could be used to explain the significant capacity of the pillared matrices to quantify the adsorption, with a significant advantage of the Langmuir model. From it the quantification of the adsorption capacities of zinc ions in the structure can be evaluated and also the possibility to obtain the constant, which expresses the bonding energy [26–30].

Metal bonding formation with the internal pillared spaces in the clays is also favored by increasing the pillar wall surfaces of the original smectite structures, besides the external part of the pillars. This complete process of metal/clay bonding is governed by the microenvironment around those pillar bridgings, which are usually covered by basic centers. These coordination centers are formed as accessories in the pillars, due to the appearance of hydroxyl groups that still exist on the surfaces, mainly in hydration of the internal structure. Thus, the positioning and amount of hydroxyl groups in outer regions, as in lamellae borders or central structures, controls chemisorption processes [5].

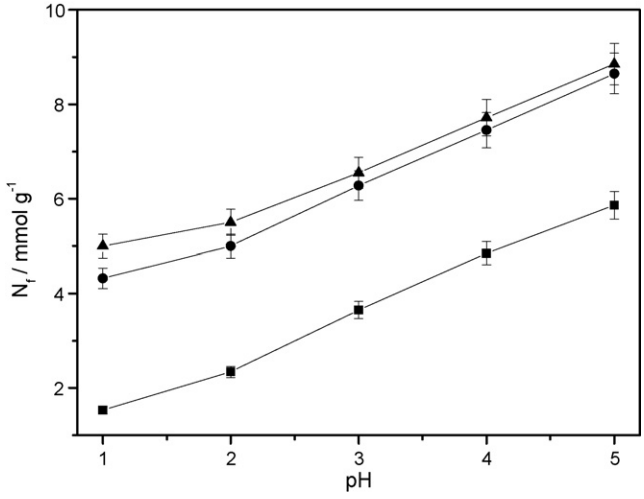

Fig. 8. Effect of pH on the adsorption of metal ions from aqueous solution (3.0 g dm^{-3} clay, initial Zn(II) concentration 50.0 mg dm^{-3}, controlled temperature 298 ± 1 K): A_1 (■), Al/Zr-A_1-723 (▲); Al/Ti-A_1-723 (●).

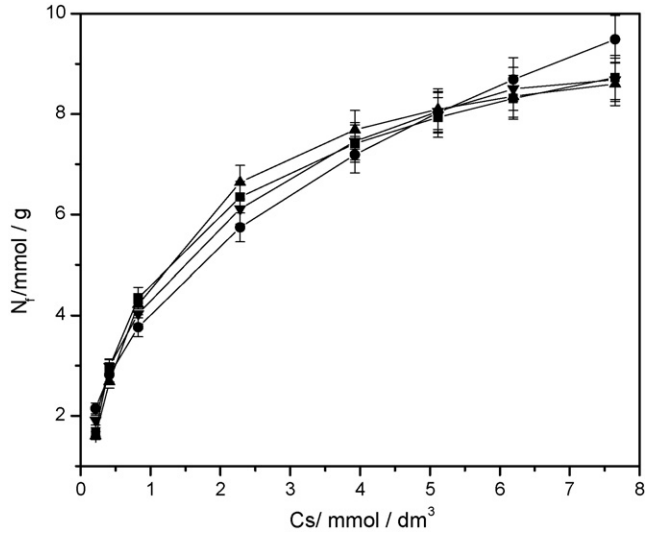

Fig. 10. The experimental data fitting for zinc (3.0 g dm^{-3} clay, initial Zn(II) concentration 50.0 mg dm^{-3}, pH 5.0, controlled temperature 298 ± 1 K) adsorption by comparing Langmuir (▲), Freundlich (●),Temkin (■) models and experimental (▼) data for Al/Zr-A_2-723.

Table 3
Langmuir, Freundlich and Temkin models applied to zinc adsorption on natural and pillared samples (clay 3.0 g dm^{-3}, initial Zn(II) 50.0 mg dm^{-3}, pH 5.0, controlled temperature 298 ± 1 K)

Sample	Langmuir			Freundlich			Temkin		
	b	K_L	r^2	K_f	N	r^2	B	A	r^2
A_1	8.576	1.0071	0.999	4.162	2.495	0.997	1.722	4.632	0.998
A_2	8.830	0.9341	0.997	4.077	2.409	0.998	1.958	4.773	0.997
Al/Zr-A_1-723	10.278	1.1198	0.999	3.476	2.155	0.999	1.859	4.312	0.996
Al/Ti-A_1-723	10.863	1.2171	0.998	3.931	2.351	0.991	2.275	4.641	0.997
Al/Zr-A_1-873	12.115	1.5012	0.997	3.178	1.933	0.998	2.203	4.185	0.997
Al/Ti-A_1-873	11.555	1.5478	0.998	3.652	1.939	0.996	2.224	4.601	0.996
Al/Zr-A_2-723	12.365	1.1518	0.997	4.035	2.001	0.998	2.287	4.500	0.999
Al/Ti-A_2-723	11.830	1.5786	0.987	4.067	2.409	0.992	1.978	4.732	0.997
Al/Zr-A_2-873	11.278	1.5879	0.999	3.666	2.155	0.958	1.899	4.373	0.995
Al/Ti-A_2-873	11.158	1.5646	0.999	3.567	2.246	0.998	1.789	4.451	0.997

3.9. Thermodynamic study

Thermodynamic studies of zinc adsorption for the pillared and the original clay samples were performed at three different temperatures, 303, 318 and 333 K. The profiles are very similar, with the adsorption increasing with the temperature, with higher values for the pillared material, up to a plateau, as shown in Fig. 11. For such adsorptions the pillared surface required activation energies and an increased temperature to ensure that more cations could overcome this energy barrier and get attached to the surface [31]. Another possibility is the creation of additional adsorption sites on the surface, arising due to dissociation of some surface components [32] at higher than room temperature, which increases the zinc uptake. These two influences may operate independently or may be simultaneous.

The thermodynamics parameters are listed in Table 4, where ΔG values were obtained by plotting $\ln K$ against $1/T$ for the Langmuir data, as shown in Fig. 12. The spontaneity of the zinc adsorption process on natural and pillared materials can be demonstrated by the negative ΔG, which increased in values with temperature for all pillared clays. For example, values varied from −0.29 to −3.35 kJ mol^{-1} for Al/Zr-A_1-723. The increase in values for each set of temperatures for a given material demonstrates that zinc is more effectively bonded to the surface, to give more pronounced ΔG values.

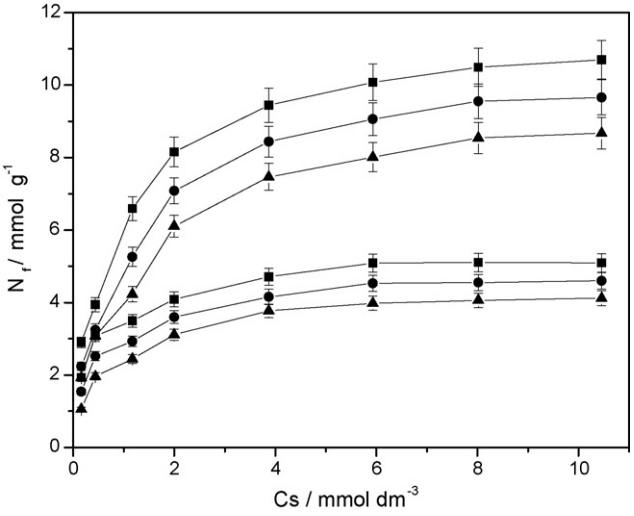

Fig. 11. N_f vs. C_s plot at 303 K (▲), 318 K (●) and 333 K (■) for A_1 and Al/Zr-A_2-723 (3.0 g dm^{-3} clay, initial Zn(II) concentration 50.0 mg dm^{-3}, pH 5.0).

The exothermic enthalpic values, varying from −24.91 to −30.69 kJ mol^{-1}, reflect the favorable affinity of zinc with the appearance of new sites, probably formed by increasing coordination sites on the external surface of pillars and the pillar-layer links. This argument can be easily visualized when these val-

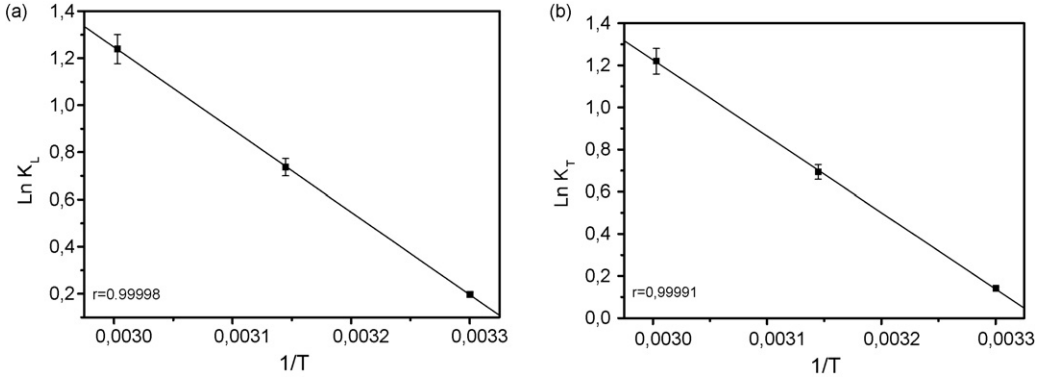

Fig. 12. $\ln K_L$ vs. $1/T$ plots Al/Ti-A_1-723 and Al/Zr-A_2-723 adsorbents (3.0 g dm^{-3} clay, initial Zn(II) concentration 50.0 mg dm^{-3}, pH 5.0).

Table 4
Thermodynamic data for adsorption of Zn(II) on natural and PILC surfaces (3.0 g dm^{-3} clay initial Zn(II) concentration 50.0 mg dm^{-3}, pH 5.0)

Sample	T (K)	K_L	$-\Delta G$ (kJ mol^{-1})	$-\Delta H$ (kJ mol^{-1})	ΔS (J K^{-1} mol^{-1})	r^2
A_1	303	1.05	0.12			
	318	1.07	0.18	2.36	7.88	0.9888
	333	1.10	0.26			
A_2	303	1.06	0.15			
	318	1.08	0.20	2.37	7.975	0.9846
	333	1.10	0.26			
Al/Zr-A_1-723	303	1.12	0.29			
	318	1.99	1.82	30.69	102.23	0.9989
	333	3.36	3.35			
Al/Ti-A_1-723	303	1.23	0.49			
	318	2.09	1.95	29.14	97.81	0.9999
	333	3.45	3.43			
Al/Zr-A_1-873	303	1.50	1.02			
	318	2.32	2.22	25.85	88.52	0.9979
	333	3.79	3.69			
Al/Ti-A_1-873	303	1.55	1.10			
	318	2.36	2.26	24.91	85.71	0.9981
	333	3.78	3.68			
Al/Zr-A_2-723	303	1.15	0.36			
	318	2.00	1.83	30.13	100.57	0.9999
	333	3.39	3.38			
Al/Ti-A_2-723	303	1.58	1.10			
	318	2.49	2.41	26.43	99.91	0.9996
	333	3.99	3.83			
Al/Zr-A_2-873	303	1.59	1.16			
	318	2.69	2.62	25.90	89.42	0.9998
	333	4.00	3.84			

ues are compared with those obtained with natural clays, with constant -2.36 kJ mol^{-1} values, which represent nearly 1/10 of those of the pillared clays. However, these results involving the pillared clays are in close agreement with similar interactions involving other heavy metal ions [31] and the magnitude of these values has been attributed to moderate bonding between zinc ions and the clay minerals [32].

Based on the spontaneity of the zinc/clay interaction at the solid/liquid interface, represented by the Gibbs free energy and the exothermic enthalpy, the entropic values were calculated and are listed in Table 4. These positive values varied from 85.71 to 102.23 J K^{-1} mol^{-1} and reflect the displacement of water molecules initially bonded to the pillared materials. The amount of solvent molecules is reinforced by the desolvation of the cation before bonding to the inorganic surface. This increase in solvent molecules in the medium is responsible for the positive entropic results [31,32]. Thus, the favorable exothermic enthalpy and the positive entropic results contributed to the spontaneity of the interactive reaction of the zinc/clay system, as expressed by the negative Gibbs free energy.

3.10. Kinetics of adsorption

Natural and pillared clays display similar behavior for zinc uptake as time increased at a fixed pH of 5.0 and a constant temperature of 298 ± 1 K. The adsorption quickly increased up to 30 min and then smoothly as the equilibrium is reached, with higher values for the pillared clays in comparison with the natural clay, as shown in Fig. 13. For all cases, the zinc uptake

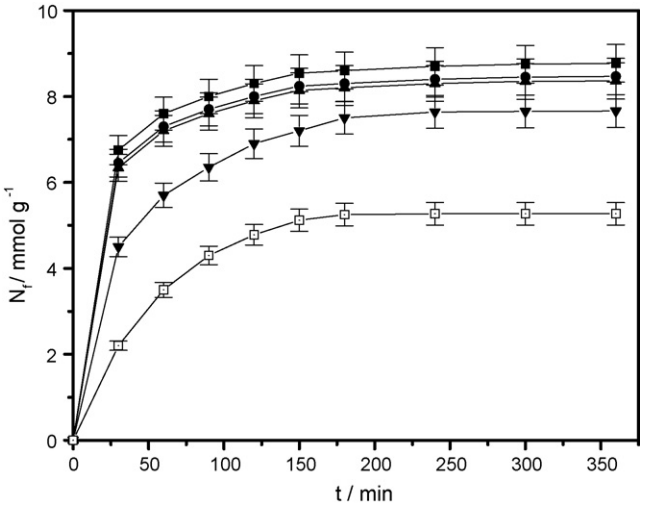

Fig. 13. Isotherms of adsorption of the natural and pillared clays with zinc (3.0 g dm^{-3} clay, initial Zn(II) concentration 50.0 mg dm^{-3}, controlled temperature 298 ± 1 K, pH 5.0): A_1 (□); Al/Zr-A_1-723 (▲); Al/Ti-A_2-723 (●); Al/Zr-A_2-723 (▼); Al/Ti-A_1-723 (■).

became almost constant after 180 min at the equilibrium condition, as demonstrated by the plateau established. During the experimental procedure the initial and final pH values were measured, without changing in value. The presence of pillars in the clay structure has resulted in a higher uptake of zinc for the same interaction time, behavior which can be attributed to the increase in the number of equivalent adsorption sites.

Some parameters are decisive in the kinetic studies of any reaction, such as temperature and concentration, to explain the mechanism of the sorption process, by using several models to fit to the experimental data [33], such as:

(a) pseudo-first-order kinetics using the Lagergren equation is generally expressed as follows [33–35]:

$$\frac{dq}{dt} = k_1(N_{eq} - N_t) \quad (7)$$

After integration and applying the boundary conditions, $N_t = 0$ for $t = 0$ and $N_t = N_t$ at $t = t$, the integrated form of Eq. (7) becomes

$$\ln(N_{eq} - N_t) = \ln N_{eq} - k_1 t \quad (8)$$

where N_{eq} and N_t are the amounts of zinc adsorbed (mmol g^{-1}) at equilibrium and at a given time t, respectively, and k_1 is the rate constant of pseudo-first-order adsorption (min^{-1}).

(b) pseudo-second-order kinetics is expressed as [34–36]:

$$\frac{dN_t}{dN_{eq}} = k_2\left(N_{eq} - N_t\right)^2 \quad (9)$$

Integrating this equation for the boundary conditions gives:

$$\frac{1}{N_{eq} - N_t} = \frac{1}{N_{eq} + k_2 t} \quad (10)$$

where k_2 is the rate constant of pseudo-second-order adsorption (min^{-1}).

(c) the useful Elovich equation [30] for energetically heterogeneous solid surface can be represented by this form:

$$N_t = \beta \ln(\alpha\beta) + \beta \ln t \quad (11)$$

where α and β, the Elovich coefficients, represent the initial adsorption rate (mmol g^{-1} min^{-1}) and the desorption coefficient (g $mmol^{-1}$), respectively.

The initial high rate for zinc adsorption, as shown in Fig. 13, may be attributed to the existence of the bare surface. However, as the coverage increases, the number of available surface sites for adsorption decreases and the rate decreases until it reaches equilibrium, when the uptake is controlled by the rate at which the adsorbed cations are transported from exterior to interior sites of the adsorbent particles [33–36].

Pseudo-first- and second-order kinetic and the Elovich models were used to check the adsorption data and the results are listed in Table 5. The values of k_1 were calculated from the plots of $\ln(N_{eq} - N_t)$ versus t, those of k_2 from t/N_t versus t; and

Table 5
Kinetic values calculated for zinc adsorption onto natural and pillared clay samples (3.0 g dm^{-3} clay, initial Zn(II) concentration 50.0 mg dm^{-3}, pH 5.0, controlled temperature 298 ± 1 K)

Sample	First-order kinetic equation			Second-order kinetic equation			Elovich equation		
	K_1 ($\times 10^2$ min^{-1})	N_{fcal} (mmol g^{-1})	r^2	K_2 ($\times 10^3$ mmol g^{-1} min^{-1})	N_{fcal} (mmol g^{-1})	r^2	α ($\times 10^3$ g $mmol^{-1}$ min^2)	β (mmol g^{-1} min^{-1})	r^2
A_1	1.73	5.52	0.9881	4.17	6.25	0.9995	9.65	1.58	0.9812
A_2	1.52	4.90	0.9876	3.98	5.30	0.9994	7.40	1.19	0.9765
Al/Zr-A_1-723	1.96	5.99	0.9767	4.88	8.33	0.9965	33.38	1.30	0.9866
Al/Ti-A_1-723	1.76	7.65	0.9741	10.51	9.06	0.9998	35.33	1.25	0.9869
Al/Zr-A_1-873	1.73	6.90	0.9845	10.69	9.12	0.9987	38.13	1.54	0.9765
Al/Ti-A_1-873	1.69	7.01	0.9812	10.38	8.97	0.9988	37.89	1.32	0.9875
Al/Zr-A_2-723	1.74	8.01	0.9785	10.42	8.75	0.9995	36.17	1.12	0.9875
Al/Ti-A_2-723	1.83	7.27	0.9858	10.43	8.65	0.9956	31.95	1.58	0.9941
Al/Zr-A_2-873	1.71	8.06	0.9878	10.15	8.78	0.9995	40.76	1.68	0.9987

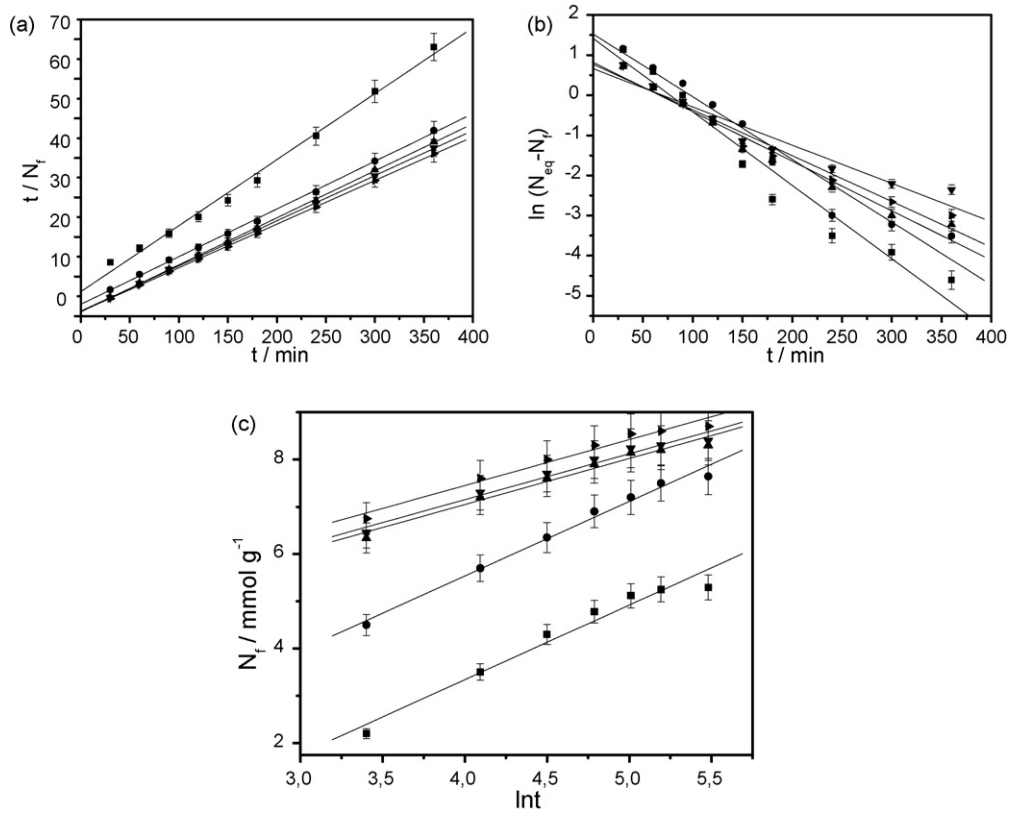

Fig. 14. Linearization of experimental data shown in Fig. 12: pseudo-second-order model (a); pseudo-first-order model (b); Elovich models (c): A_1 (■); Al/Zr-A_1-723 (●); Al/Ti-A_2-723 (▲); Al/Zr-A_2-723 (▼); Al/Ti-A_1-723 (►).

those of β and α from N_f versus ln t. The correlation coefficients for: (i) for the first-order, (ii) second-order and (iii) Elovich kinetic models are in the 0.9741–0.9881, 0.9965–0.9998 and 0.96765–0.9987 ranges, respectively. The analysis of the correlation coefficients obtained with experimental data linearization, as shown in Fig. 14, indicated that the correlation coefficients for the second-order model are higher than 0.99 and near the N_f calculated from the experimental data for this model, indicating the applicability of this kinetic equation for this system.

4. Conclusions

The X-ray powder diffraction technique confirmed an expansion of the original smectites to thermally stable d_{001} spacing from 1.55 to 2.06 nm for Al/Zr-A_1-723. For other clays the pillarization is evidenced by the increasing: (i) d_{001} distance values and (ii) the stability with high temperature at 873 K, without collapsing the inorganic structures, with advantage of these pillars in adsorbing zinc cations from aqueous solution.

Aluminum pillar formation is also confirmed through infrared spectroscopy by presenting a weak shoulder at 667 cm^{-1} with low intensity in the pillared sample spectra. Therefore, the presence of a band at 3738 cm^{-1} also confirmed the attachment of Keggin's ion in the original matrix structures.

The textural analysis is in agreement with pillared samples that were evaluated by adsorption isotherms, indicating the production of mesopore and micropore materials. The physical–chemical proprieties were optimized with the utilization of a mixed pillaring process, which can be attributed to several features: production of ions during the intercalation, entrance of them into the interlayer space and density and number of pillars.

The models used for isotherm evaluation exhibited constants similar to those obtained for experimental isotherm data. Greater variation was observed in the Freundlich model. The results obtained through linear equations are very close to those from the literature that often use a non-linear computational method based on the "Enzefitte" system. The adsorption results establish a relationship between the number of adsorbed ions and the number of acidic sites produced after the pillaring process. K_L and b values from Langmuir and Freundlich equations exhibited small variations when a plateau was formed. On the other hand, this fact implies a saturation of the acidic centers in the new smectite system produced after the pillaring process, which stabilizes the two mathematical variables that drive the process.

The maximum adsorption equilibrium was obtained when assayed up to pH 5.0, however, for such process contact time, initial concentration of cations, adsorbent quantity and temperature are also important factors to be considered. The natural and pillared clays are directly influenced by the increase in pH of the medium in the adsorption process, whose limiting factor is hydroxide formation at pH > 5.0. The kinetic studies demonstrated a straightforward equilibrium time of 180 min for zinc adsorption on pillared materials, but as a whole, the interactions could be better represented by a second-order mechanism.

Acknowledgements

The authors are indebted to CNPq for fellowships and FAPESP for financial support.

References

[1] G.W. Blindley, R.E. Sempels, Preparation and properties of some hydroxy-aluminium beidellites, Clay Clay Miner. 12 (1992) 229–237.
[2] M.L. Occelli, R.M. Tindwa, Physicochemical properties of montmorillonite interlayered with cationic oxyaluminum pillars, Clay Clay Miner. 32 (1983) 22–28.
[3] T.J. Pinnavaia, M. Tzou, S.D. Landau, On the pillaring and delamination of smectite clay catalysts by polyoxo cations of aluminum, J. Mol. Catal. 27 (1984) 195–212.
[4] S.B.C. Pergher, A. Corma, V. Fornes, Preparación y propriedades de una argila montmorillonita pilareada com polihidroxicationes de aluminio, Quim. Nova 22 (1999) 693–708.
[5] D.L. Guerra, V.P. Lemos, C. Airoldi, R.S. Angélica, Influence of the acid activation of pillared smectites from Amazon (Brazil) in adsorption process with butylamine, Polyhedron 25 (2006) 1880–2890.
[6] J.T. Kloprogge, R. Evans, L. Hicke, R.L. Frost, Characterization, Al-pillaring of smectites from Miles, Queensland (Australia), Appl. Clay Sci. 20 (2002) 157–163.
[7] P. Salerno, S. Mendioroz, Preparation of Al-pillared montmorillonite from concentrated dispersions, Appl. Clay Sci. 22 (2002) 115–123.
[8] A. Gil, M.A. Vicente, L.M. Gandia, Main factors controlling the texture of zirconia and alumina pillared clays, Micropor. Mesopor. Mater. 34 (2000) 115–125.
[9] M.R. Sun Kou, S. Mendioroz, M.L. Guijarro, A thermal study of Zr-pillared montmorillonite, Thermochim. Acta 323 (1998) 142–157.
[10] C. Volzone, Pillaring of different smectite members by chromium species (Cr-PILCs), Micropor. Mesopor. Mater. 49 (2001) 197–202.
[11] J.L. Valverde, P. Sanchez, F. Dorado, C.B. Molina, A. Romero, Influence of the synthesis conditions on the preparation of titanium-pillared clays using hydrolyzed titanium ethoxide as the pillaring agent, Micropor. Mesopor. Mater. 54 (2003) 155–165.
[12] H.L. Del Castillo, P. Grange, Preparation and catalytic activity of titanium pillared montmorillonite, Appl. Catal. A: Gen. 103 (1993) 23–34.
[13] J. Sterte, Synthesis and properties of titanium oxide cross-linked montmorillonite, Clay Clay Miner. 35 (1996) 658–664.
[14] L. Storaro, M. Lenarda, A. Rinaldi, Preparatin of hydroxy Al/Fe-pillared bentonites from concentrated clay suspensions, Micropor. Mesopor. Mater. 6 (1996) 55–63.
[15] M.L. Occelli, J.T. Hsu, L.G. Galya, Propylene oligomerization with pillared clays, J. Mol. Catal. 33 (1985) 371.
[16] K.B. Brandt, R.A. Kydd, The effect of framework substituition and pillar composition on the cracking activities of montmorillonite and beidellite, Appl. Catal. 165 (1997) 327–333.
[17] F. Gonzalez, C. Pesquera, I. Benito, E. Herrero, C. Poncio, S. Casuscelli, Pillared clay: catalytic evaluation in heavy oil cracking using a microactivity test, Appl. Catal. A: Gen. 181 (1999) 71–79.
[18] W.G. Blindley, G. Brown, Crystal structure of clay minerals and their X-ray identification, Miner. Soc. 45 (1980) 18–23.
[19] X. Tang, W.-Q. Xu, Y.-F. Shen, S.L. Suib, Study and catalytic properties of pillared clay, Chem. Mater. 7 (1995) 102.
[20] C. Airoldi, M.O. Machado, A.M. Lazarin, Thermodynamic features associated with intercalation of some *N*-alkylmonoamines into barium phosphate, J. Chem. Thermodyn. 38 (2006) 130–135.
[21] N. Yildiz, M. Erol, Z. Aktas, A. Çalimli, Adsorption of aromatic hydrocarbons on BTEA-betonites, Adsorpt. Sci. Technol. 22 (2004) 145–154.
[22] M.S. Çelik, Adsorption of ethoxylated sulfonate and nonionic on coal, J. Colloid. Interf. Sci. 129 (1989) 428–433.
[23] S. Bordoardo, F. Figueiras, E. Garrone, IR study of Brønsted acidity of Al-pillared montmorillonite, J. Catal. 147 (1994) 223–230.
[24] E.P. Barret, L.G. Joyner, P.P. Halenda, The determination of pore volume and area distribution in porous substances: I. Computation from nitrogen isotherms, J. Am. Chem. Soc. 73 (1953) 373–380.
[25] D.M. Monahar, B.F. Noeline, T.S. Anirudhan, Adsorption performance Al-Pillared bentonite clay for the removal of cobalt(II) from aqueous phase, Appl. Clay Sci. 31 (2006) 194–2006.
[26] G. Bayramoglu, S. Bektas, M.Y. Arica, Biosorption of heavy metal ions on immobilized wite-rot fungus Trametes versicolor, J. Hazard. Mater. B 101 (2003) 285–300.
[27] B. Yu, Y. Zang, A. Shukla, S.S. Shukla, K.L. Dorris, The removal of heavy metals from aqueous solution by sawdust adsorption–removal of copper, J. Hazard. Mater. B 80 (2000) 33–42.
[28] S. Yamanaka, T. Nishihara, M. Hattori, Adsorption and acidic properties of catalysts, Proc. Mater. Res. Soc. 41 (1988) 317–327.
[29] J. Ravichandran, B. Sivasankar, Proprerties and catalytic activity of acid-modified montmorillonite and vermiculite, Clay Clay Miner. 45 (1997) 854–858.
[30] K.G. Bhattacharyya, S. Sen Gupta, Pb(II) uptake by kaolinite and montmorillonite in aqueous medium: influence of activation of the clays, Colloid. Surf. A 277 (2006) 191–200.
[31] A. Kilislioglu, B. Bilgin, Thermodynamic and kinetic investigations of uranium adsorption on amberlite IR-118H resin, Appl. Radiat. Isotope 58 (2003) 155–160.
[32] S.S. Tahir, N. Rauf, Thermodynamic studies of Ni(II) adsorption onto bentonite from aqueous solution, J. Chem. Thermodyn. 35 (2003) 2003–2009.
[33] V. Gökmen, A. Serpen, Equilibrium and kinetic studies on the adsorption of dark colored compounds from apple juice using adsorbent resin, J. Food Eng. 53 (2002) 221–227.
[34] W.H. Kuan, S.-L. Lo, C.M. Chang, M.K. Wang, A geometric approach to determine adsorption and desorption kinetic constants, Chemosphere 41 (2000) 1741–1747.
[35] A.R. Cestari, E.F.S. Vieira, G.S. Vieira, L.E. Almeida, The removal of anionic dyes from aqueous solutions in the presence of anionic surfactant using aminopropylsilica—a kinetic study, J. Hazard. Mater. B 138 (2006) 133–141.
[36] M. Kithome, J.W. Paul, L.M. Lavkulich, A.A. Bomke, Kinetics of ammonium adsorption and desorption by the natural zeolite clinoptilolite, Soil Sci. Soc. Am. J. 62 (1998) 2836–2848.